Inorganic Chemistry

Article

pubs.acs.org/IC

Photoinduced Charge Transfer in Short-Distance Ferrocenylsubphthalocyanine Dyads

Pavlo V. Solntsev,[†] Katelynn L. Spurgin,[†] Jared R. Sabin,[†] Ahmed A. Heikal,[†,‡] and Victor N. Nemykin*[,†]

[†]Department of Chemistry and Biochemistry and [‡]Department of Pharmacy Practice and Pharmaceutical Sciences, University of Minnesota—Duluth, 1039 University Drive, Duluth, Minnesota 55812, United States

Supporting Information

ABSTRACT: Two new ferrocenylsubphthalocyanine dyads with ferrocenylmethoxide (**2**) and ferrocenecarboxylate (**3**) substituents directly attached to the subphthalocyanine ligand via the axial position have been prepared and characterized using NMR, UV−vis, and magnetic circular dichroism (MCD) spectroscopies as well as X-ray crystallography. The redox properties of the ferrocenyl-containing dyads **2** and **3** were investigated using the cyclic voltammetry (CV) approach and compared to those of the parent subphthalocyanine **1**. CV data reveal that the first reversible oxidation is ferrocene-centered, while the second oxidation and the first reduction are localized on the subphthalocyanine ligand. The electronic structures and nature of the optical bands observed in the UV−vis and MCD spectra of all target compounds were investigated by a density functional theory polarized continuum model (DFT-PCM) and time-dependent (TD)DFT-PCM approaches. It has been found that in both dyads the highest occupied molecular orbital (HOMO) to HOMO−2 are ferrocene-centered molecular orbitals, while HOMO−3 as well as lowest unoccupied molecular orbital (LUMO) and LUMO+1 are localized on the subphthalocyanine ligand. TDDFT-PCM data on complexes **1**−**3** are consistent with the experimental observations, which indicate the dominance of $\pi-\pi^*$ transitions in the UV−vis spectra of **1**−**3**. The excited-state dynamics of the dyads **2** and **3** were investigated using time-correlated single photon counting, which indicates that fluorescence quenching is more efficient in dyad **3** compared to dyad **2**. These fluorescence lifetime measurements were interpreted on the basis of DFT-PCM calculations.

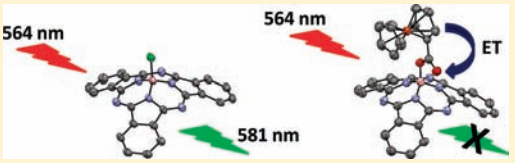

INTRODUCTION

Synthesis of functional materials with high-solar-energy conversion efficiency represents a fundamental goal in modern sciences.[1] Effective light-to-energy conversion requires the efficient formation of long-lived charge-separated (CS) electronic states, which have high energy content.[2] In natural photosynthetic systems, the sequential electron-transfer processes lead to a spatial separation of ion pairs, which follow a redox gradient created by properly aligned and electronically tuned π-congugated porphyrinoids.[3] Although a similar strategy has been successfully applied for the formation of long-lived CS states in artificial photosynthetic supramolecular multichromophoric assemblies, one serious drawback is the major loss of input energy during each electron-transfer step.[4] Simple donor−acceptor hybrids represent a very attractive alternative for the preparation of artificial photosynthetic systems.[5] In general, the electron-transfer kinetics and the excited-state relaxation mechanism in such donor−acceptor hybrids depend on the magnitude of the electronic coupling between the different substituents, which is dictated by the donor−acceptor distance, their orbital and spatial orientation, and the nature of the linking group between them.[6] In addition, charge-recombination and intermolecular interactions could also play a significant role in the kinetics of CS state formation. The most critical parameter for efficient CS state formation was shown to be the donor−acceptor distance in the assembly.[7] In particular, it has been demonstrated that a short donor−acceptor distance (~2.6 Å) favors the formation of CS states with an exceptionally long (230 μs) lifetime.[8]

Among numerous porphyrinoids used as an antenna in donor−acceptor dyads, the subphthalocyanine (SubPc) macrocycle attracted special attention because of its optical properties (very strong absorption in the visible region) and bowl-shaped geometry, which is potentially useful for covalent as well as noncovalent coordination to acceptors such as C_{60}.[9] In addition, SubPc's have higher fluorescence quantum yields and smaller reorganization energies compared to porphyrins.[10] During the past decade, Torres and co-workers as well as other groups have shown that the C_{60}−SubPc−donor triads could be used as light-harvesting subunits.[9] Specifically, they can be involved in a light-induced multistep charge transfer, which results in the formation of a spatially separated $C_{60}^{\bullet-}$−SubPc−donor$^{\bullet+}$ radical ion pair.[9] In particular, ferrocene donors, connected via a *p*-phenyloxy linker to the axial position of SubPc, provided long-lived (up to 231 μs) CS states in the above-mentioned triads.[9] It could be anticipated, however, that decreasing the ferrocene-to-SubPc distance should positively affect CS state formation. To our surprise, however, ferrocenylsubphthalocyanine dyads with a direct ferrocene−boron or substituted ferrocene−boron bond have never been investigated. Thus, in this paper, we report the synthesis,

Received: January 10, 2012
Published: May 31, 2012

   dx.doi.org/10.1021/ic3000608 | *Inorg. Chem.* 2012, 51, 6537−6547

Scheme 1

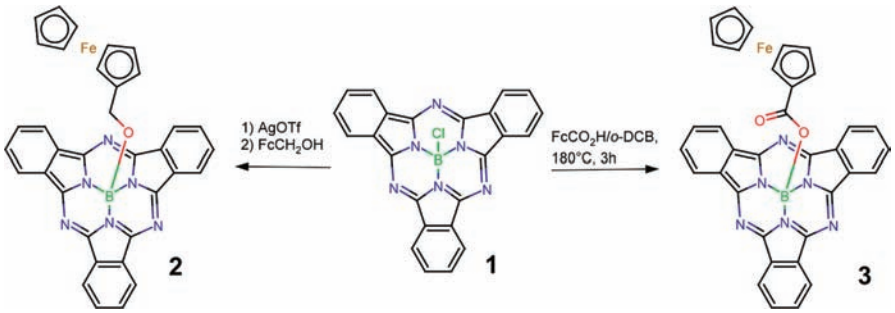

characterization, and photophysical studies of the new ferrocenylsubphthalocyanine dyads (Scheme 1) in which ferrocenylmethoxide (SubPcOCH$_2$Fc, **2**) and ferrocenecarboxylate (SubPcO$_2$CFc, **3**) are directly bonded to the boron atom in the SubPc chromophore.

EXPERIMENTAL SECTION

Reagents and materials. All reactions were performed under an argon atmosphere using standard Schlenk techniques. Solvents were purified by standard methods: tetrahydrofuran (THF) was distilled over a sodium−potassium alloy, toluene was distilled over sodium metal, dichloromethane (DCM) and hexane were distilled over calcium hydride, o-dichlorobenzene (*o*-DCB) was distilled over P_2O_5 under reduced pressure, and methanol was distilled over magnesium under an argon atmosphere. $NaBH_4$, NH_4Cl, *tert*-butyllithium solution in hexanes, SubPcCl (**1**), ferrocene, and ferrocenecarboxaldehyde were purchased from Aldrich and used without further purification. Silica gel (60 Å, 60−100 μm) was purchased from Dynamic Adsorbents Inc.

Preparation of FcCH$_2$OH (4) and FcCO$_2$H (5). The axial ligands **4**[11] and **5**[12] were prepared using slightly modified procedures reported earlier (see the Supporting Information for details).

Preparation of SubPcOCH$_2$Fc (2). A mixture of **1** (50 mg, 0.116 mmol) and silver triflate (37 mg, 0.148 mmol) was dissolved in 3 mL of dry toluene and stirred for 2.5 h at room temperature. After this period of time, a solution of **4** (50 mg, 0.233 mmol) and (*i*-Pr)$_2$NEt (20.5 μL, 0.145 mmol) in 3 mL of toluene was added as a single portion, and the reaction mixture was stirred for an additional 8 h. Solvent was removed under vacuum, and the solid was redissolved in 5 mL of DCM and loaded onto a short chromatographic column [SiO_2, toluene/THF (5:2, v/v)]. The first pink fraction was collected, its solvent was evaporated under reduced pressure, and the resulting solid was recrystallized from a water/THF mixture and then from DCM/hexane. Yield: 12 mg (17%). Elem anal. Calcd for $C_{35}H_{23}BN_6OFe{\cdot}0.12CH_2Cl_2$: C, 67.99; H, 3.78; N, 13.55. Found: C, 68.01; H, 3.83; N, 13.47. ^{1}H NMR [δ, ppm, Si(CH$_3$)$_4$, CDCl$_3$]: 8.85 (6H, dd, α-SubPc), 7.90 (6H, dd, β-SubPc), 3.75 (5H, s, Cp), 3.71 (2H, m, β-Cp), 3.40 (2H, m, α-Cp), 2.34 (2H, s, CH$_2$). ^{13}C NMR [δ, ppm, Si(CH$_3$)$_4$, CDCl$_3$]: 151.7 (α-pyrrole), 131.1 (β-pyrrole), 129.8 (α-SubPc), 122.2 (β-SubPc), 85.3 (C$_{ipso}$), 68.2 (Cp), 68.1 (α-Cp), 67.8 (β-Cp), 58.0 (CH$_2$). APCI MS (THF): 610.3 ([M]$^+$).

Preparation of SubPcO$_2$CFc (3). A mixture of ferrocenecarboxylic acid (321 mg, 1.395 mmol) and **1** (200 mg, 0.465 mmol) in 3 mL of *o*-DCB was refluxed for 3 h, cooled, and filtered, and the remaining residue was washed with DCM. Combined organic layers were evaporated under reduced pressure, and the resulting solid was redissolved in toluene and filtered. The toluene was evaporated under reduced pressure, and the remaining solid was redissolved in DCM and separated on a short chromatography column [SiO_2, DCM/THF (1:15, v/v)]. The first red fraction was collected, and the solvent was evaporated under reduced pressure. A total of 280 mg of the crude product was recrystallized first from THF/water and then from DCM/hexane. Yield: 185 mg (64%). Elem anal. Calcd for $C_{35}H_{21}BN_6O_2Fe{\cdot}0.16CH_2Cl_2{\cdot}0.21C_6H_{14}$: C, 66.69; H, 3.73; N, 12.82. Found: C, 66.77; H, 3.53; N, 12.67. ^{1}H NMR [δ, ppm, Si(CH$_3$)$_4$, CDCl$_3$]: 8.90 (6H, m, α-SubPc), 7.92 (6H, m, β-SubPc), 3.98 (2H, m, β-Cp), 3.97 (2H, m, α-Cp), 3.65 (5H, m, Cp). ^{13}C NMR [δ, ppm, Si(CH$_3$)$_4$, CDCl$_3$]: 170.47 (CO$_2$), 151.7 (α-pyrrole), 131.3 (β-pyrrole), 130.1 (α-SubPc), 122.6 (β-SubPc), 105.0 (C$_{ipso}$), 71.1 (α-Cp), 70.1 (β-Cp), 69.7 (Cp). APCI MS (THF): 624.8 ([M]$^+$).

Density Functional Theory Polarized Continuum Model (DFT-PCM) and Time-Dependent (TD)DFT-PCM Calculations. The initial geometries of complexes **1**−**3** were taken from the X-ray data and optimized at the DFT level, using a hybrid PBE1PBE exchange-correlation functional.[13] This exchange-correlation functional was shown to provide good agreement between theoretical and experimental bond distances and angles in ferrocene-containing compounds.[14] In the case of dyads **2** and **3**, the PBE1PBE exchange-correlation functional allows better agreement between theoretical and experimental geometries compared to the tested BP86 and B3LYP exchange-correlation functionals. Equilibrium geometries were confirmed by frequency calculations and specifically by the absence of imaginary frequencies. Solvation effects were modeled using the PCM approach.[15] DCM was used as the solvent in all calculations. All single-point DFT-PCM and TDDFT-PCM calculations were conducted using a pure BP86 functional,[16] which accurately describes vertical excitation energies in a variety of porphyrinoids.[17] Again, in the test calculations, the BP86 exchange-correlation functional allowed better agreement between theory and experiment compared to the tested B3LYP and PBE1PBE exchange-correlation functionals. The first 50 states were considered in all PCM-TDDFT calculations. In all cases, Wachter's full-electron basis set[18] was used for iron centers and 6-31G(d)[19] for all other atoms. All calculations were performed using *Gaussian 09* software.[20] Molecular orbital (MO) analysis was conducted using the *QMForge* program.[21]

X-ray Crystallography. Single crystals of complexes **1**−**3** suitable for X-ray crystallographic analysis were obtained by the slow evaporation of *o*-DCB, DCM/hexane, and toluene solutions, respectively. X-ray diffraction data were collected on a Rigaku RAPID-II diffractometer with a graphite monochromator using Cu Kα (λ = 1.5418 Å) or Mo Kα (λ = 0.71073 Å) radiation at −150 °C. Multiscan absorption correction[22] was applied to the data in all cases. The crystal structures were solved by a direct method (*SIR-92*)[23] and refined by a full-matrix least-squares method on F^2 using the *SHELXL-97* program.[24] The *PLATON* program was used for visualization of the results. Crystal data for complexes **1**−**3** are summarized in Table 1, while selected bond distances and angles are presented in Table 2. CCDC 861030, 861031, and 861032 contain the supplementary crystallographic data for all compounds (see the Supporting Information). These data can also be obtained free of charge via www.ccdc.cam.ac.uk/conts/retrieving.html (or from Cambridge Crystallographic Data Centre, 12 Union Road, Cambridge CB2 1EZ, U.K.; fax (+44) 1223-336-033 or e-mail deposit@ccdc.cam.ac.uk).

Spectroscopy Measurements. UV−vis data were obtained on Jasco-720 or Cary-17 spectrophotometers. Magnetic circular dichroism (MCD) data were recorded using an OLIS DCM 17 CD spectropolarimeter with a 1.4 T DeSa magnet. The MCD spectra were measured in mdeg = [θ] and converted to $\Delta\varepsilon$ (M^{-1} cm^{-1} T^{-1}) using the regular conversion formula: $\Delta\varepsilon = \theta/(32980Bdc)$, where B is the magnetic field, d is the path length, and c is the concentration.

dx.doi.org/10.1021/ic3000608 | *Inorg. Chem.* 2012, 51, 6537−6547

Table 1. Summary of Crystallographic Data for Compounds 1−3

	1	2	3
empirical formula	$C_{24}H_{12}N_6BCl$	$C_{35}H_{23}N_6OBFe$	$C_{35}H_{21}N_6O_2BFe$
fw	430.66	610.25	624.24
cryst syst	orthorhombic	monoclinic	monoclinic
space group, Z	*Pnma*, 4	*C*2/*c*, 8	$P2_1/c$, 4
a (Å)	12.1224(2)	28.610(5)	17.2645(8)
b (Å)	14.8449(10)	11.197(5)	7.7863(2)
c (Å)	10.3283(1)	18.146(5)	20.6276(14)
β (deg)	90	114.658(5)	95.019(7)
volume (Å^3)	1858.6(1)	5283(3)	2762.3(2)
ρ_{calc}(g cm^{-3})	1.539	1.535	1.501
μ (mm^{-1})	2.041[a]	0.615[b]	4.757[a]
θ_{max} (deg)	68.24[a]	27.49[b]	68.41[a]
measd/unique reflns	12595/1756	17320/6032	29594/5040
R_{int}	0.0351	0.0492	0.0647
GOF(F^2)	1.156	1.047	1.092
R1[c]/wR2[d] [$I > 2\sigma(I)$]	0.0668/0.1872	0.0612/0.1553	0.0657/0.1817
R1[c]/wR2[d] (all data)	0.0852/0.2127	0.0704/0.1625	0.0815/0.2060
$\Delta\rho_{max}/\Delta\rho_{min}$ (e Å^{-3})	0.838/−0.485	1.067/−0.902	0.618/−0.971

[a]Cu Kα. [b]Mo Kα. [c]$R1(F) = \sum||F_o| - |F_c||/\sum|F_o|$. [d]$wR2(F^2) = \{\sum[w(F_o^2 - F_c^2)^2]/\sum w(F_o^2)^2]\}^{1/2}$.

Complete spectra were recorded at room temperature in parallel and antiparallel directions with respect to the magnetic field. APCI mass spectrometry (MS) data were collected using a Agilent LCQ MS system and THF as the solvent. Electrochemical measurements were conducted using a CH Instruments electrochemical analyzer utilizing a three-electrode scheme with platinum working, auxiliary, and Ag/AgCl reference electrodes in a 0.1 M solution of tetrabutylammonium perchlorate (TBAP) in *N*,*N*-dimethylformamide (DMF) with redox potentials corrected using an internal standard (decamethylferrocene, Fc*) in all cases. The redox potentials were then corrected to ferrocene using appropriate oxidation potentials for Fc^*/Fc^{*+} vs Fc/Fc^+ in the DMF/TBAP system. NMR spectra were recorded on a Varian INOVA instrument with a 500 MHz frequency for protons and 125 MHz for carbon. Chemical shifts are reported in parts per million (ppm) and referenced to tetramethylsilane [$Si(CH_3)_4$] as an internal standard. In all cases, final assignments of ^{1}H and ^{13}C signals were made using COSY and HMQC spectra. Elemental analyses were conducted by Atlantic Microlab. Steady-state fluorescence data were collected using a Cary Eclipse fluorimeter at room temperature.

Time-resolved fluorescence data measurements were carried out using a time-correlated single-photon-counting (TCSPC) technique, which was described in detail elsewhere.[25] Briefly, femtosecond laser pulses (475 nm, 4.2 MHz, 120 fs) were generated using a titanium−sapphire laser system (950 nm, 760 MHz, Mira 900-F, Coherent), a pulse picker (Mira 9200, Coherent), and a second-harmonic generator for one-photon excitation of compounds **1**−**3**. The samples were prepared in a deep-well slide and a coverslip, sealed with nail polish, and positioned in the focal plane of a 1.2NA microscope objective (Olympus) in an inverted IX81 microscope (Olympus). The epifluorescence signal was directed toward a microchannel plate photomultiplier tube (MCP-PMT; R3809U, Hamamatsu) through a filter (585 ± 40 nm) and a Glan-Thompson polarizer, which was set at the magic angle (54.7°). A histogram of fluorescence photon arrival times (i.e., a fluorescence decay) was recorded using a SPC 830 module (Becker and Hickl, Berlin, Germany) and analyzed using *SPCImage* software.

Table 2. Selected Bond Lengths (Å) and Angles (deg) for Compounds 1−3

Compound 1			
Cl1−B1	1.890(6)	N2−B1	1.470(8)
N1−B1	1.473(4)		
N2−B1−N1	105.7(3)	N2−B1−Cl1	112.4(4)
N1−B1−N1#1[a]	106.5(4)	N1−B1−Cl1	113.0(3)
Compound 2			
Fe···π[b](centroid)	1.650(2), 1.659(2)	N1−B1	1.504(4)
Fe···C(average)	2.049(2)	N3−B1	1.499(4)
C25−O1	1.398(4)	N5−B1	1.489(4)
C25−C26	1.497(4)	O1−B1	1.430(4)
O1−B1−N5	111.1(2)	O1−B1−N1	118.1(2)
O1−B1−N3	116.0(2)	N5−B1−N1	104.3(2)
N5−B1−N3	103.1(2)	N3−B1−N1	102.7(2)
C26−C25−O1−B1	−160.9(2)	O1−C25−C26−C27	148.1(3)
Compound 3			
Fe···π[b](centroid)	1.644(2), 1.648(2)	N1−B1	1.498(5)
Fe···C(average)	2.039(2)	N3−B1	1.490(5)
B1−O1	1.467(4)	N5−B1	1.480(5)
B1−O2	2.772(5)	O2−C25	1.218(4)
C25−C26	1.472(5)	O1−C25	1.334(4)
O2−C25−O1	123.1(3)	O1−B1−N3	117.7(3)
O2−C25−C26	124.8(4)	N5−B1−N3	104.5(3)
C25−O1−B1	121.3(3)	N5−B1−N1	104.9(3)
O1−B1−N1	115.1(3)	N3−B1−N1	104.8(3)
O1−C25−C26−C27	10.7(5)	B1−O1−C25−C26	178.0(3)

[a]#1: x, $^3/_2 - y$, z. [b]Ring centroids were built on C26−C27−C28−C29−C30 and C31−C32−C33−C34−C35.

RESULTS AND DISCUSSION

Synthesis. Ferrocenylmethanol and ferrocenecarboxylic acid were prepared in multigram quantities using slightly modified reported methods (Supporting Information, Scheme S1).[11,12] Ferrocenyl-containing SubPc dyads **2** and **3** were synthesized as described in Scheme 1. Nucleophilic substitution of the chloride atom by alkoxide (OR^-) in SubPcBCl or SubPcBBr can be achieved by refluxing these macrocycles with a corresponding alcohol in toluene.[26] While this approach is very simple, it is effective only for the thermally stable alcohols. In the case of the reaction between **1** and **4** in boiling toluene, no desired $SubPcBOCH_2Fc$ was detected. Instead, bis-(ferrocenylmethylene) ether, $(FcCH_2)O$, and unreacted **1** were isolated under these reaction conditions. In order to obtain complex **2**, we adopted a new versatile two-step strategy described by Torres and co-workers for axial modification of the **1** systems.[27] First, an anion-exchange reaction between **1** and silver triflate was conducted, followed by quenching of the resulting SubPcOTf by ferrocenylmethanol. Using this strategy, subphthalocyanine **2** was obtained in 17% yield (Scheme 1). The relatively low yield originates from the low stability of complex **2** on silica gel that was required for its successful purification.

The introduction of a carboxylic acid group into SubPc systems is not straightforward. Indeed, only SubPc's axially

dx.doi.org/10.1021/ic3000608 | *Inorg. Chem.* 2012, 51, 6537−6547

bonded to acetate, phenylacetate, trifluoroacetate, trichloroacetate, chloroacetate, and benzoate have been described so far.[28] Moreover, synthetic procedures for the preparation of these complexes require boiling or melting of **1** with the corresponding acid. This method, however, is unacceptable in the case of ferrocenecarboxylic acid because of its well-known thermal decomposition.[29] We found, however, that substitution of the axial chlorine atom in SubPcBCl by ferrocenecarboxylate could be achieved by refluxing the reagents in *o*-DCB for 3 h (Scheme 1).

X-ray Crystal Structures. An ultimate knowledge on the chemical structures of ferrocenylsubphthalocyanine dyads **2** and **3** was further gained from single-crystal X-ray analysis. In order to accurately compare structural changes in complexes **2** and **3** to the parent SubPc **1**, an X-ray structure of compound **1** was also determined with the same experimental conditions. Refinement parameters for compounds **1**−**3** are presented in Table 1, while their selected bond lengths and angles are summarized in Table 2. ORTEP diagrams of compounds **1**−**3** are shown in Figure 1. Similar to all previously known structures of SubPc complexes,[9,26−28,30] the macrocyclic ligand adopts a bowl-shaped conformation, with the boron atom pointing away from the macrocyclic base. In all structures, the boron atoms are located in a trigonal-pyramidal (3N + Cl for **1** and 3N + O for **2** and **3**) environment. The axial B−Cl bond in **1** is longer, while the B−O bonds in **2** and **3** are shorter compared to the B−N bonds in respective SubPc's. The B−O bonds in dyads **2** [1.430(4) Å] and **3** [1.467(4) Å] are quite different but similar to the other SubPc's with alkoxy or carboxy substituents in axial positions.[9,26−28,30] The shorter B−O bond distance in dyad **2** can be understood in terms of the electron-donating properties of the axial ligand in this compound. The η^1 coordination of the axial ferrocenecarboxylate group in dyad **3** could be clearly determined from its X-ray structure (Figure 1 and Table 2). Indeed, the B−O1 and B−O2 bond distances are 1.467(4) and 2.772(5) Å, respectively, while the O1−C25 and O2−C25 bond distances are 1.334(4) and 1.218(4) Å, respectively. This is indicative of the η^1 coordination of the axial ferrocenecarboxylate group and the presence of C−O and C═O bonds in **3**. The axial ferrocene ligands are tilted toward one of the nitrogen atoms, which is reflected in the respective O−B−N angles [118.1(2)°, 116.0(2)°, and 111.1(2)° in **2** and 108.6(3)°, 117.7(3)°, and 115.1(3)° in **3**]. The B−N bond distances in dyads **2** and **3** are close to each other but longer than those in the parent compound **1** [1.489(4)−1.504(4) Å in **2** and 1.480(5)−1.498(5) Å in **3**]. The O−C bond distance in **2** [1.398(4) Å] is significantly shorter than the same bond distance in **4** [for three symmetry-unique molecules of **4**: 1.434(6), 1.451(6), and 1.450(5) Å],[11] which is indicative of the electron-acceptor properties of the SubPc macrocycle. Torsion angles B1−O1−C25−C26 and O1−C25−C26−C27 in dyad **2** are −160.9(2)° and 148.1(3)°, respectively, while those in dyad **3** are 178.0(3)° and 10.7(5)°, respectively. The carboxylic acid group in **3** is almost coplanar with the monosubstituted cyclopentadienyl (Cp) ring [torsion angle O1−C25−C26−C27 is 10.7(5)°]. The Fe−C bond distances were observed in the ranges of 2.031(3)−2.070(3) and 2.016(4)−2.071(4) Å in dyads **2** and **3**, respectively, and the Cp rings adopt close to an eclipsed conformation. The packing motif in dyads **2** and **3** is very similar and consists of $\pi\cdots\pi$ stacking between overlapping isoindole fragments of the macrocyclic ligand (Supporting Information, Figures S1 and S2). To the contrary, $\pi\cdots\pi$ stacking in the parent SubPc **1** occurs between the isoindole fragment of one molecule and the *meso*-nitrogen-containing six-membered fragment of the neighboring macrocycle (Supporting Information, Figure S3). Both of these motifs are typical for substituted SubPc's.[9,26−28,30]

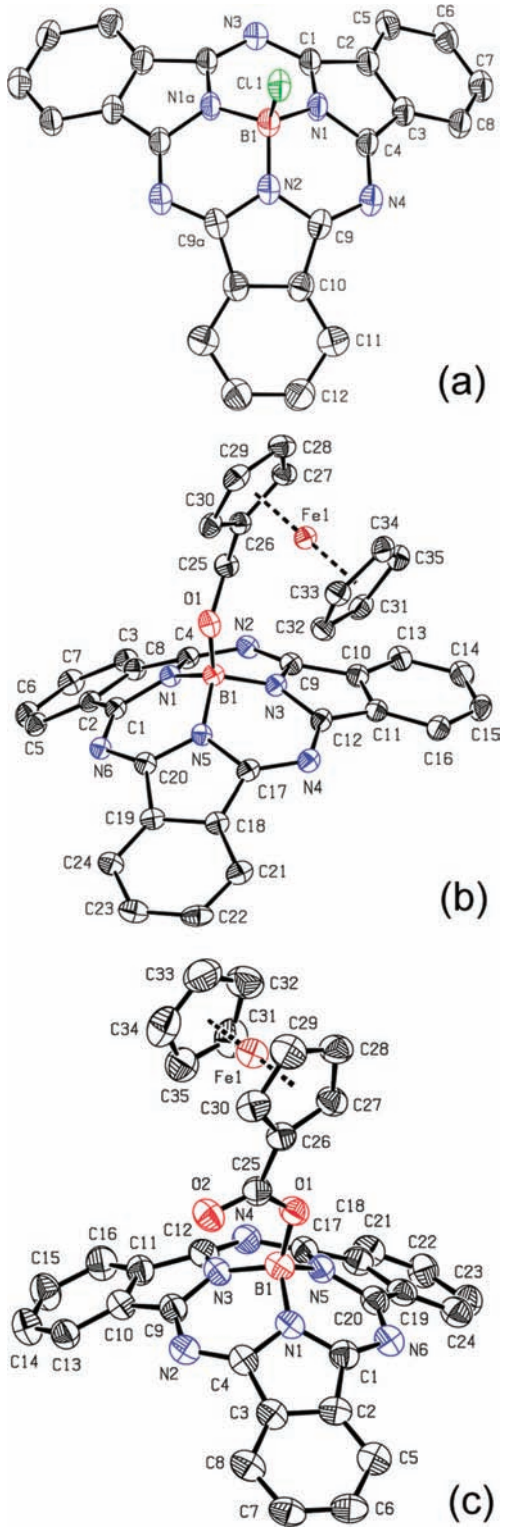

Figure 1. ORTEP-labeled diagram for X-ray structures of **1** (a), **2** (b), and **3** (c). All hydrogen atoms are omitted for clarity. Thermal ellipsoid probability level of 50%.

NMR Spectroscopy. The introduction of ferrocenyl substituents into target complexes **2** and **3** significantly

dx.doi.org/10.1021/ic3000608 | *Inorg. Chem.* 2012, 51, 6537−6547

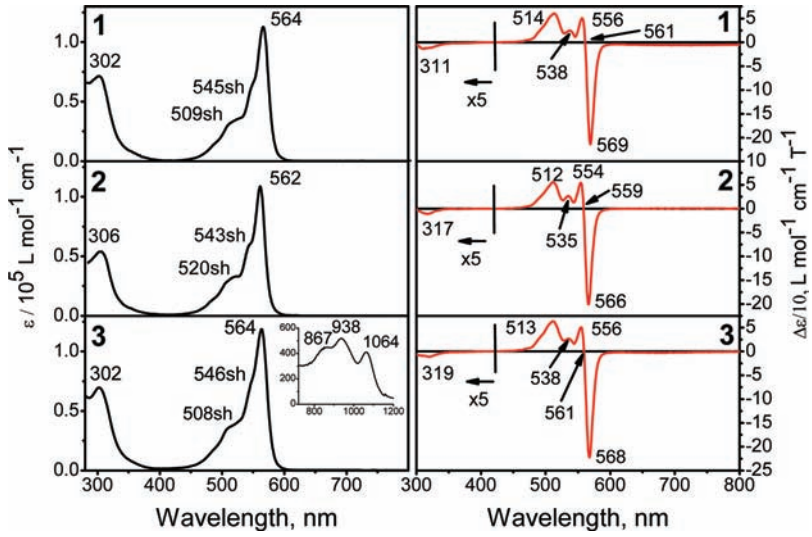

Figure 2. UV−vis (left) and MCD (right) spectra of **1**−**3** .

Table 3. UV−Vis Absorption and Emission Data for Compounds 1−3

	UV−vis	fluorescence			
compound	λ_{abs}, nm (log ε)	λ_{fl}, nm	τ_1, ns (%)	τ_2, ps (%)	τ_{av}, ps
1	564 (5.05), 545sh (4.79), 509sh (4.56), 302 (4.86)	581	3.11 (100)		3110
2	562 (5.04), 543sh (4.77), 520sh (4.52), 306 (4.73)	578	2.92 (30)	5 (70)	882
3	564 (5.07), 546sh (4.86), 508sh (4.58), 302 (4.84)	580[a]	1.65 (3)	21 (97)	65

[a]Crude estimation because of the low emission intensity.

increases their solubility in common organic solvents compared to the parent macrocycle **1**. Indeed, both complexes **2** and **3** are reasonably soluble in toluene, DCM, chloroform, and THF. Substitution of the axial chloride in **1** by ferrocenylmethoxide and ferrocenecarboxylate was easily confirmed by ^{1}H NMR spectroscopy. Similar to other axially coordinated phthalocyanines and their analogues,[31] the ^{1}H NMR spectra of complexes **2** and **3** exhibit proton signals of the Cp ligands that are shifted to higher fields compared with the corresponding signals observed in parents **4** and **5** (Supporting Information, Figures S4 and S5). The effects of the ring current are especially significant for protons located close to the macrocycle. Indeed, protons of the $-CH_2-$ group in complex **2** have a resulting shift in their resonance from 4.33 to 2.34 ppm. As expected, NMR signals of the ferrocenyl protons are less shifted compared to the NMR signals of the parent molecules. It is interesting to note that the chemical shifts of the α-Cp and β-Cp protons in complex **3** are very close to each other and cannot be separated in the COSY experiment, although their integral intensity is in good agreement with the proposed structure. NMR shifts for the SubPc aromatic protons in all complexes are close to each other, suggesting a negligible influence of the axial ligand on the chemical shifts. A similar trend was observed in the case of other axially substituted SubPc's.[9,26−28]

UV−Vis and MCD Spectroscopy of SubPc's 1−3. UV−vis and MCD spectra of SubPc's **1**−**3** are presented in Figure 2 and summarized in Table 3. In agreement with previous studies,[9,26−28,32] axial substitution of the chlorine atom by alkoxy or carboxylate ligands in SubPc's **2** and **3** has a negligible effect on their UV−vis and MCD spectra, which are dominated by the very intense intraligand $\pi-\pi^*$ transitions. Indeed, the low-energy Q band is observed at 564 nm in parent SubPc **1** and ferrocenylsubphthalocyanine dyad **3**, while only a 2 nm shift in the Q-band position is observed for complex **2**. Similarly, the MCD spectra of complexes **2** and **3** are almost indistinguishable from the MCD spectrum of parent SubPc **1**. They are dominated by the Faraday *A* term centered at 559 nm (complex **2**) and 561 nm (complex **3**), which corresponds to the most intense Q-band band in the UV−vis spectra of these compounds and confirms their 3-fold effective symmetry.

As shown below, our electrochemical experiments as well as DFT-PCM and TDDFT-PCM calculations predict that ferrocene-centered MOs in dyads **2** and **3** should dominate the highest occupied molecular orbital (HOMO) region. As a result, we explored the possible presence of metal-to-ligand charge-transfer (MLCT) transitions in the near-IR (NIR) region. Although MLCT bands were not observed in dyad **2** between 600 and 1500 nm, three relatively low intensity bands centered at 867, 938, and 1064 nm were observed for several independently prepared samples of dyad **3** (Figure 2). These weak MLCT transitions could be attributed to charge transfer from ferrocene-centered HOMO to HOMO−2 to the nearly degenerate SubPc-centered lowest unoccupied molecular orbital (LUMO) and LUMO+1 on the basis of TDDFT-PCM calculations, as discussed below. The absence of similar MLCT bands in dyad **2** can be understood in terms of the higher flexibility of the axial ferrocene-containing substituent, which could result in significantly lower band intensities, and thus MLCT bands could be masked by the low-energy wing of the intense ($\varepsilon \sim 100000$) Q band. The MCD signals for NIR MLCT bands even at the solubility and/or optical saturation limits are extremely weak, which is typical for MLCT transitions in ferrocenyl-containing donor−acceptor dyads.[33]

Redox Properties. The redox properties of the ferrocenylsubphthalocyanine dyads were examined using cyclic

dx.doi.org/10.1021/ic3000608 | Inorg. Chem. 2012, 51, 6537−6547

voltammetry (CV) approach (Table 4). Because of the relatively low solubility of dyads **2** and **3** and especially the parent SubPc **1** in DCM and THF, all electrochemical experiments were conducted in a DMF/TBAP system. The ferrocene substituents in dyads **2** and **3** exhibit reversible first oxidations at +0.02 and +0.35 V (Figure 3). Oxidation of the axial ferrocenyl substituent in dyad **2** was observed at a lower potential compared with dyad **3**, which is in good agreement with the electron-donating nature of the ferrocenylmethanol group and DFT calculations presented below. All three studied SubPc's (**1**–**3**) reveal a single reduction peak, at −1.70, −1.51, and −1.32 V, respectively, which correspond to the one-electron-reduction process centered at the macrocyclic ligand. In agreement with previous reports,[9,26−28,34] oxidation of the SubPc ligand was observed as the only partially reversible process at 0.66, 0.55, and 0.73 V, for complexes **1**–**3**, respectively, which is attributed to partial degradation of the macrocyclic ligand. Degradation of the macrocyclic ligand was further confirmed by CV experiments on dyad **3**. Indeed, when the CV experiments were conducted between 0 and −1.75 V, only a single reversible peak of SubPc reduction was observed at −1.32 V (Figure 3). On the other hand, when the CV experiment was conducted by sweeping between +1.25 and −1.75 V, four additional peaks at −0.043, −0.337, −0.698, and −0.958 V were observed. Similar peaks, assigned to the degradation of SubPc's, have been reported previously.[34] It is important to note that the difference between the oxidation and reduction potentials of the SubPc core was ∼2 V in all three systems, which is in the typical range for all SubPc's.

Table 4. Redox Properties of Compounds 1−3

	oxidation, V		reduction, V
	E^{Ox2}	$E_{1/2}{}^{Ox1}$(Fc)	$E_{1/2}{}^{R1}$
1	0.655[a]		−1.698[a]
2	0.545[a]	0.020	−1.505
3	0.725[a]	0.345	−1.323

[a]Irreversible process; all potentials (±5 mV) are given in volts relative to Fc/Fc^+.

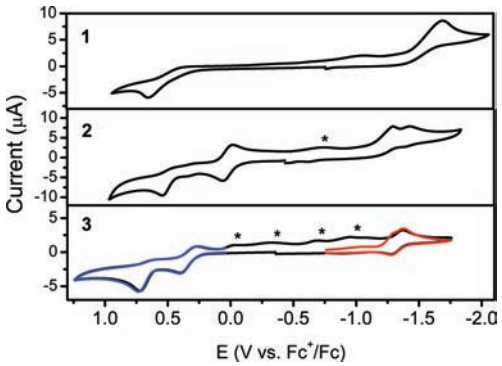

Figure 3. Room temperature CV data for compounds **1**–**3** in the DMF/TBAP system (asterisks indicate that the macrocycle degradation products originated from the irreversible oxidation of the SubPc core).

Fluorescence Quantum Yield and Excited-State Lifetime. Axially substituted SubPc's are known as fluorescent emitters with electron- and/or energy-donating or -accepting capabilities.[10] The high fluorescence quantum yield (Φ_F) of the parent SubPc **1** (Φ_F = 0.25) allows for study of the intramolecular excited-state deactivation process. Indeed, the Q-band excitation of the parent compound **1** exhibits an intense emission centered at 581 nm, assigned to the $S_1 \rightarrow S_0$ transition in the SubPc ligand (Figure 4). The luminescence observed in SubPc's has shown to be the mirror image of the Q-band and is almost independent of the solvent as well as the nature of the axial substituents. When fluorescence spectra for compounds **1**–**3** were recorded under the same experimental conditions (i.e., concentration, excitation wavelength and intensity, and resolution), both emission intensities in dyads **2** and **3** were found to be several orders of magnitude lower than the fluorescence observed in **1**. Such strong quenching of the fluorescence, however, has no effect on the overall emission profile for compounds **1**–**3** (Figure 4 and Table 3). Such behavior has been observed for several SubPc's with different quenching groups and was attributed to the intrinsically faster singlet excited-state deactivation.[9,10] In order to examine this tentative assignment, we have measured the first excited-state lifetimes of compounds **1**–**3** using the TCSPC approach.[25]

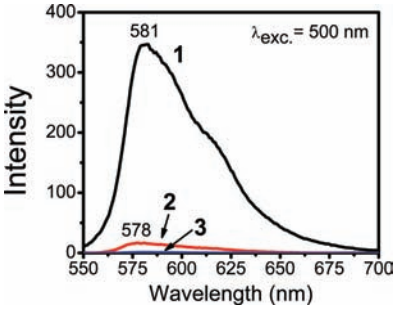

Figure 4. Comparative fluorescence intensities of compounds **1**–**3** recorded at the same optical density at 500 nm. The excitation wavelength in all cases was 500 nm.

The S_1 fluorescence of the parent **1** excited at 475 nm and detected at 585 ± 40 nm decays as a single exponent with an estimated fluorescence lifetime of τ_{S1} = 3.11 ns. In contrast, the S_1 state fluorescence of ferrocenyl-containing dyads **2** and **3** decays as a biexponential, as summarized in Table 3. More importantly, the dominant component in the fluorescence decay of ferrocenyl-containing dyads **2** and **3** was found to be 5 ps (70%) and 21 ps (97%), respectively. It is worth noting that these ultrafast decay components are faster than the full-width half-maximum (fwhm) of our system response function (∼45 ps), which was used in the deconvolution-based fitting algorithm. The observed ultrafast fluorescence lifetimes of complexes **2** and **3** confirm the presence of efficient deactivation processes, which are assigned as charge transfer. These fluorescence lifetime measurements are, therefore, in general agreement with our UV−vis and electrochemical data as well as TDDFT-PCM calculations presented below.

DFT-PCM and TDDFT-PCM Calculations. Further insights into the electronic structure, spectroscopy, and redox properties of the ferrocene-containing dyads **2** and **3** were gained using DFT-PCM and TDDFT-PCM calculations, which provide accurate energetic and spectroscopic parameters for a large variety of ferrocene-containing complexes[35] and macrocyclic compounds including SubPc's.[17,36] As shown in Table 5, the predicted geometries from DFT-PCM calculations are in good agreement with the X-ray experimental parameters. The DFT-PCM predicted MO energy diagrams for SubPc's **1**–**3** are

dx.doi.org/10.1021/ic3000608 | Inorg. Chem. 2012, 51, 6537−6547

Table 5. Comparison of the Experimental and DFT-PCM-Predicted Bond Distances in Compounds 1−3

bond	X-ray	DFT-PCM
	Compound **1**[a]	
B−Cl	1.890(6)	1.855
B−N	1.473(4); 1.470(8)	1.485
	Compound **2**[b]	
B−O	1.430(4)	1.416
B−N	1.498(5); 1.490(5); 1.480(5)	1.508, 1.508, 1.496
C−O	1.398(4)	1.408
	Compound **3**[b]	
B−O	1.467(4)	1.458
B−N	1.498(5); 1.490(5); 1.480(5)	1.494, 1.494, 1.491
C−O	1.334(4)	1.337
C O	1.218(4)	1.216

[a]The C_{3v} point group was used during geometry optimization by DFT, and local C_s symmetry was observed in the solid state. [b]The C_1 point group was used during geometry optimization.

presented in Figure 5, while an analysis of the orbital compositions is provided in Figure 6 and the Supporting

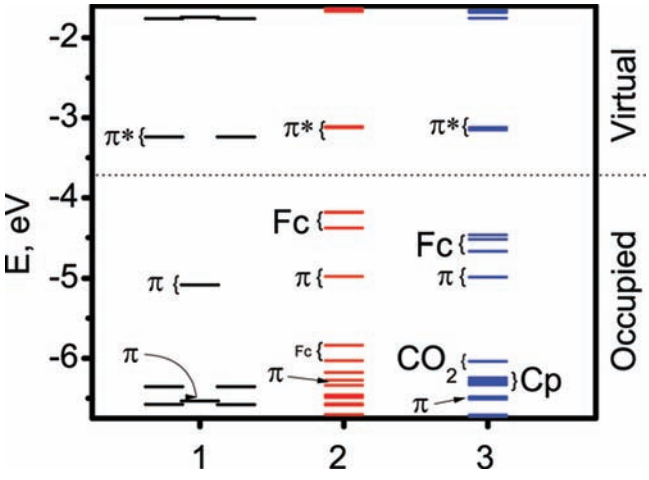

Figure 5. DFT-PCM-predicted MO energy diagram for compounds **1**−**3**.

Information, Table S1. In addition, the frontier orbitals of the target SubPc complexes **1**−**3** are pictured in Figure 7. In agreement with Gouterman's classic four-orbital model for porphyrins and phthalocyanines,[37] the HOMO in the parent **1** has a_2 symmetry (C_{3v} point group) and is a SubPc-centered π orbital with an electron density distribution that resembles an a_{1u} MO in the phthalocyanine's D_{4h} point group. In agreement with previous calculations on SubPc's[36] but contrary to closed-shell phthalocyanines and porphyrins,[38] HOMO−1 and HOMO−2 are doubly degenerate MOs, which, as predicted by TDDFT-PCM calculations, contribute significantly to the B-band region intensity of the UV−vis spectrum of **1**. The HOMO−3 again resembles a classic Gouterman's MO with a large contribution from the *meso*-nitrogen atoms (Figure 7). The introduction of axial ferrocenyl-containing ligands in dyads **2** and **3** leads to the situation where HOMO to HOMO−2 become predominantly iron-centered MOs (d_{xy}, $d_{x^2-y^2}$, and d_{z^2}, respectively) entirely localized on the axial organometallic ligands (Figure 7), with all occupied SubPc-centered π orbitals having lower energies. Such a MO description is in excellent

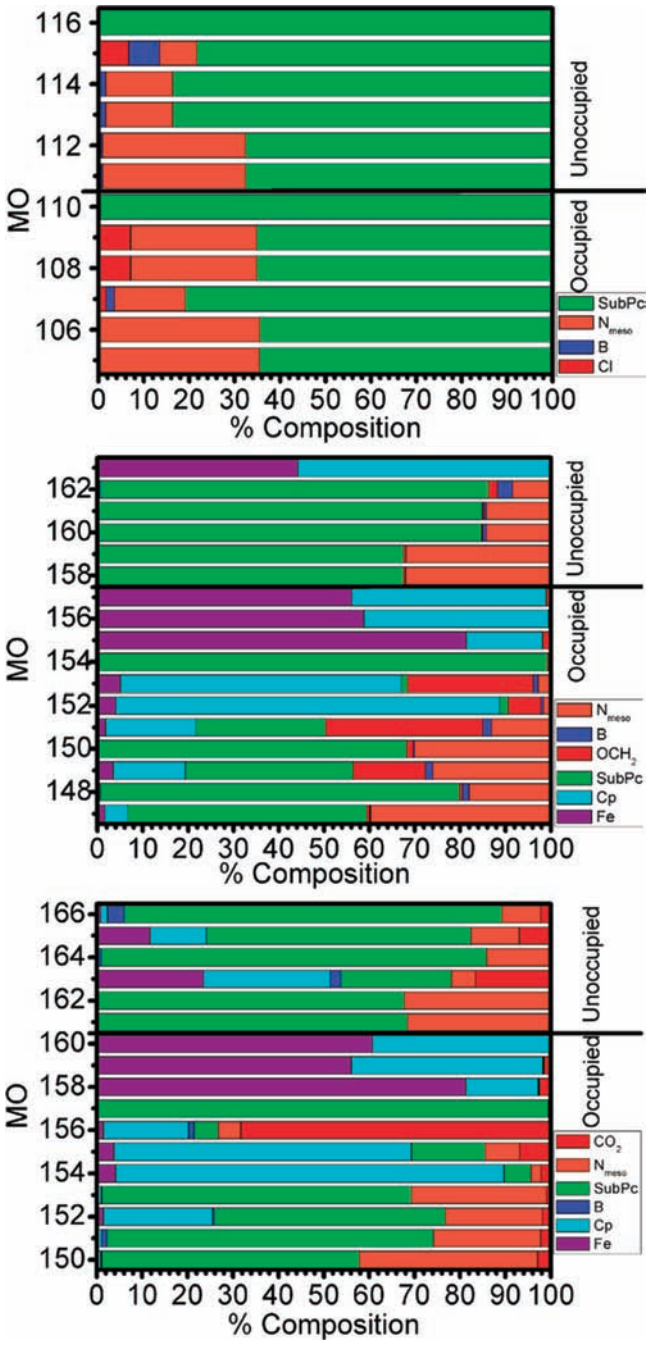

Figure 6. MO compositions of compounds **1**−**3** predicted at the DFT-PCM level.

agreement with the electrochemical data, which suggest that the first oxidation process in dyads **2** and **3** is ferrocene-centered. As expected from the electron-withdrawing nature of the carboxylic group, the ferrocenyl-centered HOMO to HOMO−2 in dyad **3** are more stable (−4.466, −4.522, and −4.664 eV) compared to analogous MOs in dyad **2** (−4.180, −4.187, and −4.378 eV). In all investigated SubPc's, LUMO and LUMO+1 are, or nearly are, doubly degenerate π^* MOs entirely localized on the SubPc ligand. These MOs are well separated from the higher energy unoccupied orbitals.

DFT-PCM calculations suggest that the UV−vis spectrum of the parent compound **1** would be dominated by the symmetry-allowed $\pi-\pi^*$ transitions, while in the case of the dyads **2** and **3**, additional low-energy, low-intensity HOMO to HOMO−2

dx.doi.org/10.1021/ic3000608 | *Inorg. Chem.* 2012, 51, 6537−6547

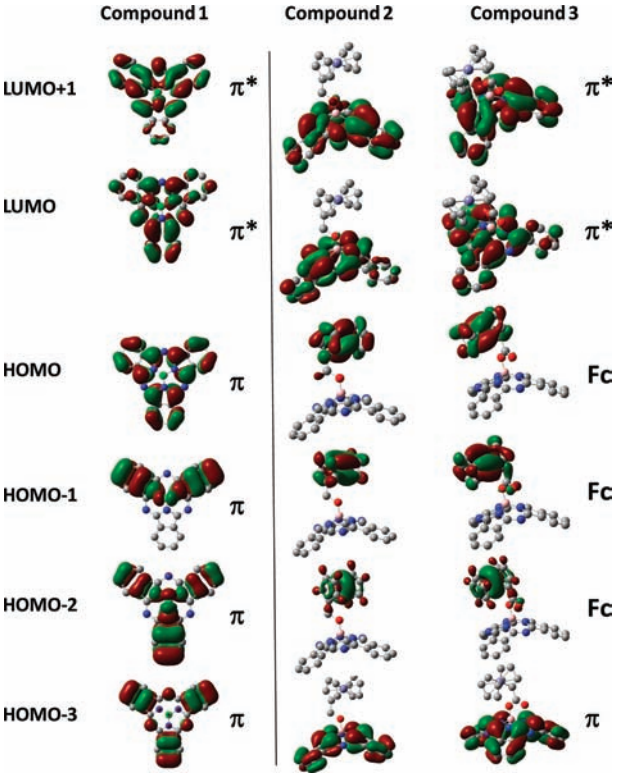

Figure 7. DFT-PCM-predicted frontier orbitals of compounds **1**–**3**.

→ LUMO, LUMO+1 MLCT transitions are expected in their UV–vis spectra. Further insight into the nature of the experimentally observed transitions was gained using the TDDFT-PCM approach. It was found that TDDFT-PCM calculations reproduce well all experimentally observed features in the SubPc complexes **1**–**3** (Figures 8–10 show the

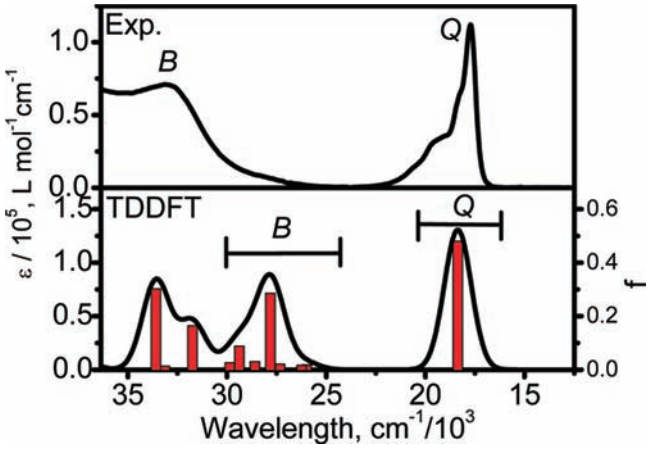

Figure 8. Experimental (top) and TDDFT-PCM-predicted (bottom) UV–vis spectra of compound **1**. The Q- and B-band regions are labeled as Q and B.

experimental and TDDFT-PCM-predicted data in the reciprocal centimeter scale, while similar data in the nanometer scale are presented in the Supporting Information, Figures S6–S8; expansion coefficients for all transitions are presented in the Supporting Information, Tables S2–S4). In agreement with earlier publications,[17,36,39] typical TDDFT-PCM errors for complexes **1**–**3** are in the very reasonable range of ~0.1–0.2

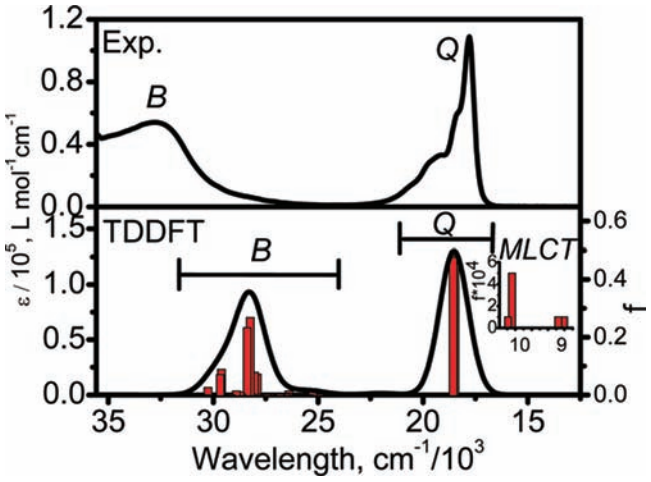

Figure 9. Experimental (top) and TDDFT-PCM-predicted (bottom) UV–vis spectra of complex **2**. Q- and B-band and MLCT regions are labeled as Q, B, and MLCT.

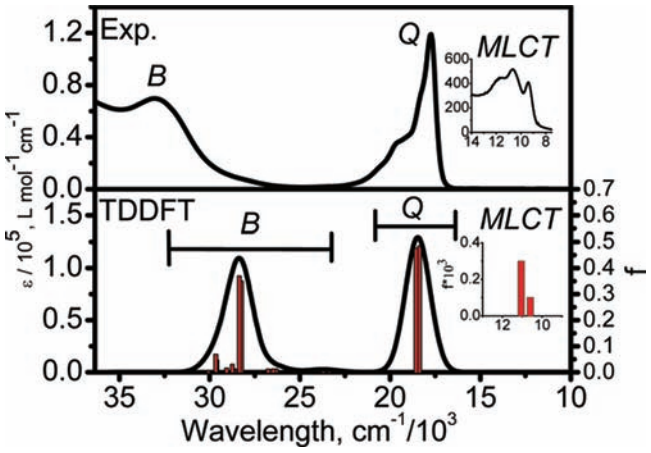

Figure 10. Experimental (top) and TDDFT-PCM-predicted (bottom) UV–vis spectra of complex **3**. Q- and B-band and MLCT regions are labeled as Q, B, and MLCT.

eV. All features in the TDDFT-PCM-calculated spectra of parent SubPc **1** could be arranged in two regions, as labeled in Figure 8, while those calculated for dyads **2** and **3** could be arranged in three spectral regions, as labeled in Figures 9 and 10. In agreement with previous calculations, the Q-band region in complexes **1**–**3** could be entirely described by the two SubPc-centered π–π^* transitions originating from HOMO → LUMO, LUMO+1 (complex **1**) or HOMO-3 → LUMO, LUMO+1 (complexes **2** and **3**). Similarly, the B-band region in SubPc's **1**–**3** is described by several SubPc-centered π–π^* transitions dominated by Gouterman-type transitions from HOMO–3 → LUMO, LUMO+1 (complex **1**) or HOMO–9 → LUMO, LUMO+1 (complexes **2** and **3**). In addition to Q- and B-band regions, the MLCT region was predicted by the TDDFT-PCM calculations in the NIR area for ferrocene-containing dyads **2** and **3** (Figures 9 and 10). The MLCT region originates from the six ferrocene-centered HOMO to HOMO–2 → LUMO, LUMO+1 transitions, which are predicted to have a several orders of magnitude lower intensity than the SubPc-centered π–π^* transitions. Both TDDFT-PCM-predicted intensities for MLCT transitions and their relative energies (i.e., lower energies for complex **2** compared to

dx.doi.org/10.1021/ic3000608 | Inorg. Chem. 2012, 51, 6537–6547

those of complex **3**) are in a good agreement with the experimental data. In general, TDDFT-PCM data correlate very well with the experimental data although, in all cases, the calculated excitation energies for the Q-band and MLCT regions are slightly overestimated, while those for the B-band region are slightly underestimated.

The DFT-PCM and TDDFT-PCM calculations explain the observed differences in the fluorescence lifetime measurements for dyads **2** and **3** as well as the relatively large fluorescence yield of dyad **2** compared with that in dyad **3**. Although the excited-state lifetime of both dyads **2** and **3** is shorter than that of the parent SubPc **1**, the average lifetime for the S_1 excited state in more rigid dyad **3** is more than 100 times shorter than that in the more flexible dyad **2** (Table 3). A rational explanation of this phenomenon could be achieved by detailed analysis of the electronic structures and nature of the excited states of dyads **2** and **3**. Taking into consideration TDDFT-PCM calculations and earlier data on SubPc's, it is reasonable to expect that the S_1 excited state in dyads **2** and **3** predominantly originates from the SubPc-centered $\pi \rightarrow \pi^*$ transitions (i.e., HOMO−3 → LUMO, LUMO+1; Figures 5 and 7). Once the S_1 state has been formed, nonradiative electron transfer from the ferrocene substituent to the half-filled HOMO−3 forms the CS state ($SubPc^{\bullet-}$-Fc^{+}), observed and characterized earlier by the femtosecond regime transient absorption measurements for several ferrocene-containing SubPc's[9] (Figure 11). The

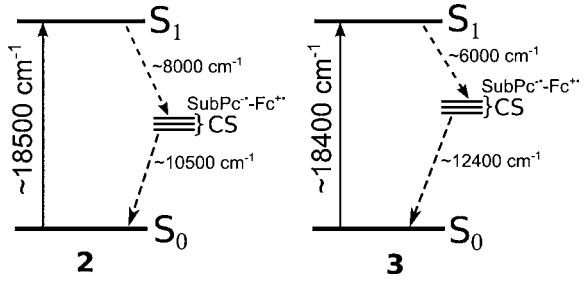

Figure 11. Proposed nonradiative deactivation mechanism of the S_1 state in dyads **2** and **3**.

formation of CS states will be especially efficient when the energy difference between the energies of S_1 and CS is small. According to TDDFT-PCM and electrochemical data, the S_1 and CS states in dyad **3** are energetically much closer to each other compared to those in dyad **2**. Thus, we can speculate that the S_1 state couples with the CS states through a vibronic coupling mechanism,[40] which is more efficient for dyad **3** than dyad **2**. Accordingly, the average lifetime of the S_1 state in dyad **3** should be shorter compared to that in dyad **2**, which is in agreement with our experimental data. The observed long average lifetime of the S_1 state in dyad **2** is consistent with the relatively higher fluorescence yield in this complex compared to that in dyad **3**.

CONCLUSIONS

In this report, we synthesized two new ferrocenylsubphthalocyanine dyads with ferrocenylmethoxide (**2**) and ferrocenecarboxylate (**3**) substituents directly attached to the SubPc ligand via the axial position. New dyads were characterized using NMR, UV−vis, and MCD spectroscopies as well as X-ray crystallography. The X-ray crystallographies of **2** and **3** confirmed the trigonal-pyramidal geometry of the boron centers and an axial coordination of the ferrocene substituents to the parent macrocycle. The redox properties of ferrocenyl-containing dyads **2** and **3** were investigated using the CV approach and compared to those in parent SubPc **1**. It was found that the first reversible oxidation is ferrocene-centered, while the second oxidation and first reduction are localized on the SubPc ligand. The electronic structures and nature of the electronic transitions observed in UV−vis and MCD spectra of all target compounds were also confirmed using DFT-PCM and TDDFT-PCM calculations. It has been found that in dyads **2** and **3** HOMO to HOMO−2 are ferrocene-centered MOs, while HOMO−3 as well as LUMO and LUMO+1 have π or π^* nature and are localized on the SubPc macrocycle. The excitation energies calculated using the TDDFT-PCM approach in complexes **1**−**3** are consistent with the experimental data and clearly suggest the dominance of π−π^* transitions in the UV−vis spectra of **1**−**3**. In addition, several weak MLCT bands were predicted by the TDDFT-PCM calculations in the NIR region of the UV−vis spectra of dyads **2** and **3**. The steady-state and time-resolved fluorescence of dyads **2** and **3** indicate that fluorescence quenching is more efficient in dyad **3** than in dyad **2**, which is in agreement with DFT-PCM and TDDFT-PCM calculations. Our results represent a first step toward a rational design of new donor−acceptor dyads that are potentially useful in light-harvesting elements.

ASSOCIATED CONTENT

Supporting Information

CIF files for complexes **1**−**3**, DFT-PCM-optimized coordinates and complete set of TDDFT-PCM-predicted expansion coefficients for compounds **1**−**3**, experimental and TDDFT-PCM-predicted UV−vis spectra of complexes **1**−**3** in nanometer scale, tabulated DFT-PCM MO compositions for compounds **1**−**3**. This material is available free of charge via the Internet at http://pubs.acs.org.

AUTHOR INFORMATION

Corresponding Author

*E-mail: vnemykin@d.umn.edu.

Notes

The authors declare no competing financial interest.

ACKNOWLEDGMENTS

Generous support from NSF Grant CHE-1110455 and NSF MRI Grant CHE-0922366, the Minnesota Supercomputing Institute to V.N.N., and a University of Minnesota UROP grant to J.R.S. is greatly appreciated. Additional support was provided by NSF (MCB0718741) and NIH (AG030949) grants (to A.A.H.).

REFERENCES

(1) (a) Sun, Y.; Welch, G. C.; Leong, W. L.; Takacs, C. J.; Bazan, G. C.; Heeger, A. J. *Nat. Mater.* **2012**, *11*, 44−48. (b) Whittell, G. R.; Hager, M. D.; Schubert, U. S.; Manners, I. *Nat. Mater.* **2011**, *10*, 176−188. (c) *Electron Transfer in Chemistry*; Balzani, V., Ed.; Wiley-VCH: Weinheim, Germany, 2001; Vols. *I*−*V*. (d) Melkozernov, A. N.; Barber, J.; Blankenship, R. E. *Biochemistry* **2006**, *45*, 331−345. (e) Guenes, S.; Neugebauer, H.; Sariciftci, N. S. *Chem. Rev.* **2007**, *107*, 1324−1338.

(2) (a) Imahori, H.; Mori, Y.; Matano, Y. *J. Photochem. Photobiol. C* **2003**, *4*, 51−83. (b) Imahori, H.; Tamaki, K.; Araki, Y.; Sekiguchi, Y.; Ito, O.; Sakata, Y.; Fukuzumi, S. *J. Am. Chem. Soc.* **2002**, *124*, 5165−5174. (c) D'Souza, F.; Chitta, R.; Gadde, S.; Islam, D.-M. S.; Schumacher, A. L.; Zandler, M. E.; Araki, Y.; Ito, O. *J. Phys. Chem. B*

2006, *110*, 25240−25250. (d) Springer, J.; Kodis, G.; De La Garza, L.; Moore, A. L.; Moore, T. A.; Gust, D. *J. Phys. Chem. A* **2003**, *107*, 3567−3575. (e) González-Rodríguez, D.; Bottari, G. *J. Porphyrins Phthalocyanines* **2009**, *13*, 624−636.

(3) *Molecular Mechanisms of Photosynthesis*; Blankenship, R. E., Ed.; Blackwell Science: Malden, MA, 2002.

(4) (a) Aratani, N.; Osuka, A. In *Handbook of Porphyrin Science*; Kadish, K. M., Smith, K. M., Guilard, R., Eds.; World Scientific Publishing Co. Pte. Ltd.: Hackensack, NJ, 2010; Vol. *1*, pp 1−132. (b) Balaban, T. S. In *Handbook of Porphyrin Science*; Kadish, K. M., Smith, K. M., Guilard, R., Eds.; World Scientific Publishing Co. Pte. Ltd.: Hackensack, NJ, 2010; Vol. *1*, pp 221−306. (c) Zhao, Z.; Cammidge, A. N.; Cook, M. J. *Chem. Commun.* **2009**, 7530−7532.

(5) (a) Yoon, Z. S.; Yang, J.; Yoo, H.; Cho, S.; Kim, D. In *Handbook of Porphyrin Science*; Kadish, K. M., Smith, K. M., Guilard, R., Eds.; World Scientific Publishing Co. Pte. Ltd.: Hackensack, NJ, 2010; Vol. *1*, pp 439−506. (b) Gonzalez-Rodriguez, D.; Carbonell, E.; Rojas, G. M.; Castellanos, C. A.; Guldi, D. M.; Torres, T. *J. Am. Chem. Soc.* **2010**, *132*, 16488−16500. (c) El-Khouly, M. E.; Shim, S. H.; Araki, Y.; Ito, O.; Kay, K.-Y. *J. Phys. Chem. B* **2008**, *112*, 3910−3917. (d) Solntsev, P. V.; Sabin, J. R.; Dammer, S. J.; Gerasimchuk, N. N.; Nemykin, V. N. *Chem. Commun.* **2010**, 6581−6583. (e) Ziessel, R.; Ulrich, G.; Elliott, K. J.; Harriman, A. *Chem.—Eur. J.* **2009**, *15*, 4980−4984. (f) Mauldin, C. E.; Piliego, C.; Poulsen, D.; Unruh, D. A.; Woo, C.; Ma, B.; Mynar, J. L.; Frechet, J. M. J. *ACS Appl. Mater. Interfaces* **2010**, *2*, 2833−2838. (g) Gonzalez-Rodriguez, D.; Torres, T.; Olmstead, M. M.; Rivera, J.; Angeles Herranz, M.; Echegoyen, L.; Atienza Castellanos, C.; Guldi, D. M. *J. Am. Chem. Soc.* **2006**, *128*, 10680−10681.

(6) (a) Grimm, B.; Hausmann, A.; Kahnt, A.; Seitz, W.; Spanig, F.; Guldi, D. M. In *Handbook of Porphyrin Science*; Kadish, K. M., Smith, K. M., Guilard, R., Eds.; World Scientific Publishing Co. Pte. Ltd.: Hackensack, NJ, 2010; Vol. *1*, pp 133−220. (b) Araki, Y.; Ito, O. *J. Photochem. Photobiol. C* **2008**, *9*, 93−110. (c) Guldi, D. M.; Hirsch, A.; Scheloske, M.; Dietel, E.; Troisi, A.; Zerbetto, F.; Prato, M. *Chem.—Eur. J.* **2003**, *9*, 4968−4979. (d) Albinsson, B.; Eng, M. P.; Pettersson, K.; Winters, M. U. *Phys. Chem. Chem. Phys.* **2007**, *9*, 5847−5864. (e) Nieto, C. R.; Guilleme, J.; Villegas, C.; Delgado, J. L.; Gonzalez-Rodriguez, D.; Martin, N.; Torres, T.; Guldi, D. M. *J. Mater. Chem.* **2011**, *21*, 15914−15918. (f) Rohde, G. T.; Sabin, J. R.; Barrett, C. D.; Nemykin, V. N. *New J. Chem.* **2011**, *35*, 1440−1448. (g) Nemykin, V. N.; Rohde, G. T.; Barrett, C. D.; Hadt, R. G.; Sabin, J. R.; Reina, G.; Galloni, P.; Floris, B. *Inorg. Chem.* **2010**, *49*, 7497−7509. (h) Nemykin, V. N.; Rohde, G. T.; Barrett, C. D.; Hadt, R. G.; Bizzarri, C.; Galloni, P.; Floris, B.; Nowik, I.; Herber, R. H.; Marrani, A. G.; Zanoni, R.; Loim, N. M. *J. Am. Chem. Soc.* **2009**, *131*, 14969−14978. (i) Nemykin, V. N.; Galloni, P.; Floris, B.; Barrett, C. D.; Hadt, R. G.; Subbotin, R. I.; Marrani, A. G.; Zanoni, R.; Loim, N. M. *Dalton Trans.* **2008**, 4233−4246. (j) Nemykin, V. N.; Barrett, C. D.; Hadt, R. G.; Subbotin, R. I.; Maximov, A. Y.; Polshin, E. V.; Koposov, A. Y. *Dalton Trans.* **2007**, 3378−3389. (k) Vecchi, A.; Gatto, E.; Floris, B.; Conte, V.; Venanzi, M.; Nemykin, V. N.; Galloni, P. *Chem. Commun.* **2012**, *48*, 5145−5147.

(7) (a) D'Souza, F.; Ito, O. In *Handbook of Porphyrin Science*; Kadish, K. M., Smith, K. M., Guilard, R., Eds.; World Scientific Publishing Co. Pte. Ltd.: Hackensack, NJ, 2010; Vol. *1*, pp 307−438. (b) El-Khouly, M. E.; Ito, O.; Smith, P. M.; D'Souza, F. *J. Photochem. Photobiol., C* **2004**, *5*, 79−104. (c) Fukuzumi, S. *Phys. Chem. Chem. Phys.* **2008**, *10*, 2283−2297. (d) D'Souza, F.; Ito, O. *Organic Electronics and Photonics*; Nalwa, H. R., Ed.; American Scientific Publishers: Stevenson Ranch, CA, 2008; Vol. *1*, Chapter 13. (e) Ohkubo, K.; Fukuzumi, S. *Bull. Chem. Soc. Jpn.* **2009**, *82*, 303−315.

(8) Ohkubo, K.; Kotani, H.; Shao, J.; Ou, Z.; Kadish, K. M.; Li, G.; Pandey, R. K.; Fujitsuka, M.; Ito, O.; Imahori, H.; Fukuzumi, S. *Angew. Chem., Int. Ed.* **2004**, *43*, 853−856.

(9) (a) Verreet, B.; Rand, B. P.; Cheyns, D.; Hadipour, A.; Aernouts, T.; Heremans, P.; Medina, A.; Claessens, C. G.; Torres, T. *Adv. Energy Mater.* **2011**, *1*, 565−568. (b) Luhman, W. A.; Holmes, R. J. *Adv. Funct. Mater.* **2011**, *21*, 764−771. (c) Shimizu, S.; Nakano, S.; Hosoya, T.; Kobayashi, N. *Chem. Commun.* **2011**, *47*, 316−318. (d) Gonzalez-Rodriguez, D.; Carbonell, E.; Guldi, D. M.; Torres, T. *Angew. Chem., Int. Ed.* **2009**, *48*, 8032−8036. (e) Verreet, B.; Schols, S.; Cheyns, D.; Rand, B. P.; Gommans, H.; Aernouts, T.; Heremans, P.; Genoe, J. *J. Mater. Chem.* **2009**, *19*, 5295−5297. (f) Gonzalez-Rodriguez, D.; Torres, T.; Herranz, M. A.; Echegoyen, L.; Carbonell, E.; Guldi, D. M. *Chem.—Eur. J.* **2008**, *14*, 7670−7679. (g) Kim, J.-H.; El-Khouly, M. E.; Araki, Y.; Ito, O.; Kay, K.-Y. *Chem. Lett.* **2008**, *37*, 544−545. (h) Iglesias, R. S.; Claessens, C. G.; Rahman, G. M. A.; Herranz, M. A.; Guldi, D. M.; Torres, T. *Tetrahedron* **2007**, *63*, 12396−12404. (i) Claessens, C. G.; Gonzalez-Rodriguez, D.; Iglesias, R. S.; Torres, T. *C. R. Chimie* **2006**, *9*, 1094−1099. (j) Claessens, C. G.; Torres, T. *Chem. Commun.* **2004**, 1298−1299. (k) Gonzalez-Rodriguez, D.; Torres, T.; Guldi, D. M.; Rivera, J.; Herranz, M. A.; Echegoyen, L. *J. Am. Chem. Soc.* **2004**, *126*, 6301−6313.

(10) (a) Wrobel, D.; Boguta, A.; Mazurkiewicz, P. *Spectrochim. Acta A* **2003**, *59*, 2841−54. (b) Kobayashi, N. *J. Chem. Soc., Chem. Commun.* **1991**, 1203−1205. (c) Yanagi, H.; Mukai, H.; Nair, M. *Thin Solid Films* **2006**, *499*, 123−128. (d) Xu, S.; Chen, K.; Tian, H. *J. Mater. Chem.* **2005**, *15*, 2676−2680. (e) Gonzalez-Rodriguez, D.; Claessens, C. G.; Torres, T.; Liu, S.; Echegoyen, L.; Vila, N.; Nonell, S. *Chem.—Eur. J.* **2005**, *11*, 3881−3893. (f) Ohno-Okumura, E.; Sakamoto, K.; Kato, T.; Hatano, T.; Fukui, K.; Karatsu, T.; Kitamura, A.; Urano, T. *Dyes Pigm.* **2002**, *53*, 57−65. (g) Rahman, G. M. A.; Lueders, D.; Rodriguez-Morgade, M. S.; Caballero, E.; Torres, T.; Guldi, D. M. *ChemSusChem* **2009**, *2*, 330−335. (h) Xu, H.; Ng, D. K. P. *Chem.—Asian J.* **2009**, *4*, 104−110. (i) Diaz, D. D.; Bolink, H. J.; Cappelli, L.; Claessens, C. G.; Coronado, E.; Torres, T. *Tetrahedron Lett.* **2007**, *48*, 4657−4660. (j) Geyer, M.; Plenzig, F.; Rauschnabel, J.; Hanack, M.; Del Rey, B.; Sastre, A.; Torres, T. *Synthesis* **1996**, 1139−1151. (k) Medina, A.; Claessens, C. G.; Rahman, G. M. A.; Lamsabhi, A. M.; Mo, O.; Yanez, M.; Guldi, D. M.; Torres, T. *Chem. Commun.* **2008**, 1759−1761. (l) Xu, H.; Jiang, X.-J.; Chan, E. Y. M.; Fong, W.-P.; Ng, D. K. P. *Org. Biomol. Chem.* **2007**, *5*, 3987−3992.

(11) Bellouard, F.; Chuburu, F.; Yaouanc, J.-J.; Handel, H.; Le Mest, Y. *New J. Chem.* **1999**, *23*, 1133−1135.

(12) Goldberg, S. I.; Keith, L. H.; Prokopov, T. S. *J. Org. Chem.* **1963**, *28*, 850−851.

(13) (a) Adamo, C.; Barone, V. *J. Chem. Phys.* **1999**, *110*, 6158−6169. (b) Perdew, J. P.; Burke, K.; Ernzerhof, M. *Phys. Rev. Lett.* **1996**, *77*, 3865−3868. (c) Perdew, J. P.; Burke, K.; Ernzerhof, M. *Phys. Rev. Lett.* **1997**, *78*, 1396−1396.

(14) (a) Firme, C. L.; Pontes, D. de L.; Antunes, O. A. C. *Chem. Phys. Lett.* **2010**, *499*, 193−198. (b) Kalamse, V.; Wadnerkar, N.; Chaudhari, A. *J. Phys. Chem. C* **2010**, *114*, 4704−4709. (c) Meylemans, H. A.; Damrauer, N. H. *Inorg. Chem.* **2009**, *48*, 11161−11175. (d) Alparone, A.; Reis, H.; Papadopoulos, M. G. *J. Phys. Chem. A* **2006**, *110*, 5909−5918. (e) Solntsev, P. V.; Dudkin, S. V.; Sabin, J. R.; Nemykin, V. N. *Organometallics* **2011**, *30*, 3037−3046.

(15) Tomasi, J.; Mennucci, B.; Cammi, R. *Chem. Rev.* **2005**, *105*, 2999−3093.

(16) (a) Becke, A. D. *Phys. Rev. A* **1988**, *38*, 3098−3100. (b) Perdew, J. P. *Phys. Rev. B* **1986**, *33*, 8822−8824.

(17) (a) Nemykin, V. N.; Hadt, R. G. *J. Phys. Chem. A* **2010**, *114*, 12062−12066. (b) Nemykin, V. N.; Hadt, R. G.; Belosludov, R. V.; Mizuseki, H.; Kawazoe, Y. *J. Phys. Chem. A* **2007**, *111*, 12901−12913. (c) Zhang, L.; Qi, D.; Zhang, Y.; Bian, Y.; Jiang, J. *J. Mol. Graph. Model.* **2011**, *29*, 717−725. (d) Zarate, X.; Schott, E.; Arratia-Perez, R. *Int. J. Quantum Chem.* **2011**, *111*, 4186−4196. (e) Soldatova, A. V.; Kim, J.-H.; Rizzoli, C.; Kenney, M. E.; Rodgers, M. A. J.; Rosa, A.; Ricciardi, G. *Inorg. Chem.* **2011**, *50*, 1135−1149. (f) Ricciardi, G.; Soldatova, A. V.; Rosa, A. *J. Porphyrins Phthalocyanines* **2010**, *14*, 689−700.

(18) Wachters, A. J. H. *J. Chem. Phys.* **1970**, *52*, 1033−1036.

(19) McLean, A. D.; Chandler, G. S. *J. Chem. Phys.* **1980**, *72*, 5639−5648.

(20) Frisch, M. J.; Trucks, G. W.; Schlegel, H. B.; Scuseria, G. E.; Robb, M. A.; Cheeseman, J. R.; Scalmani, G.; Barone, V.; Mennucci, B.; Petersson, G. A.; Nakatsuji, H.; Caricato, M.; Li, X.; Hratchian, H. P.; Izmaylov, A. F.; Bloino, J.; Zheng, G.; Sonnenberg, J. L.; Hada, M.; Ehara, M.; Toyota, K.; Fukuda, R.; Hasegawa, J.; Ishida, M.; Nakajima,

T.; Honda, Y.; Kitao, O.; Nakai, H.; Vreven, T.; Montgomery, J. A., Jr.; Peralta, J. E.; Ogliaro, F.; Bearpark, M.; Heyd, J. J.; Brothers, E.; Kudin, K. N.; Staroverov, V. N.; Kobayashi, R.; Normand, J.; Raghavachari, K.; Rendell, A.; Burant, J. C.; Iyengar, S. S.; Tomasi, J.; Cossi, M.; Rega, N.; Millam, N. J.; Klene, M.; Knox, J. E.; Cross, J. B.; Bakken, V.; Adamo, C.; Jaramillo, J.; Gomperts, R.; Stratmann, R. E.; Yazyev, O.; Austin, A. J.; Cammi, R.; Pomelli, C.; Ochterski, J. W.; Martin, R. L.; Morokuma, K.; Zakrzewski, V. G.; Voth, G. A.; Salvador, P.; Dannenberg, J. J.; Dapprich, S.; Daniels, A. D.; Farkas, Ö.; Foresman, J. B.; Ortiz, J. V.; Cioslowski, J.; Fox, D. J. *Gaussian 09*, revision A.1; Gaussian, Inc.: Wallingford, CT, 2009.

(21) Tenderholt, A. L. *QMForge*, version 2.1; Stanford University: Stanford, CA, 2011.

(22) Otwinowski, Z.; Minor, W. In *Methods in Enzymology*; Carter, C. W., Jr., Sweet, R. M.,Eds.; Academic Press: New York, 1997; Vol. *276*, pp 307−326.

(23) Altomare, A.; Cascarano, G.; Giacovazzo, C.; Guagliardi, A.; Burla, M. C.; Polidori, G.; Camalli, M. *J. Appl. Crystallogr.* **1994**, *27*, 435.

(24) Sheldrick, G. M. *Acta Crystallogr.* **2008**, *A64*, 112−122.

(25) (a) Yu, Q.; Proia, M.; Heikal, A. A. *J. Biomed. Opt.* **2008**, *13*, 041315. (b) Heikal, A. A. In *Advances in Planar Lipid Bilayers and Liposomes*; Iglic, A., Ed.; Elsevier, Inc.: New York, 2011; Vol. *13*, pp 169−197.

(26) (a) Del Rey, B.; Keller, U.; Torres, T.; Rojo, G.; Agullo-Lopez, F.; Nonell, S.; Marti, C.; Brasselet, S.; Ledoux, I.; Zyss, J. *J. Am. Chem. Soc.* **1998**, *120*, 12808−12817. (b) Kasuga, K.; Idehara, T.; Handa, M.; Ueda, Y.; Fujiwara, T.; Isa, K. *Bull. Chem. Soc. Jpn.* **1996**, *69*, 2559−2563. (c) Gonzalez-Rodriguez, D.; Torres, T.; Denardin, E. L. G.; Samios, D.; Stefani, V.; Correa, D. S. *J. Organomet. Chem.* **2009**, *694*, 1617−1622. (d) Morse, G. E.; Paton, A. S.; Lough, A.; Bender, T. P. *Dalton Trans.* **2010**, 3915−3922. (e) Lapok, L.; Claessens, C. G.; Woehrle, D.; Torres, T. *Tetrahedron Lett.* **2009**, *50*, 2041−2044. (f) Claessens, C. G.; Gonzalez-Rodriguez, D.; del Rey, B.; Torres, T.; Mark, G.; Schuchmann, H.-P.; von Sonntag, C.; MacDonald, J. G.; Nohr, R. S. *Eur. J. Org. Chem.* **2003**, 2547−2551.

(27) Guilleme, J.; Gonzalez-Rodriguez, D.; Torres, T. *Angew. Chem., Int. Ed.* **2011**, *50*, 3506−3509.

(28) Potz, R.; Goldner, M.; Huckstadt, H.; Cornelissen, U.; Tutass, A.; Homborg, H. *Z. Anorg. Allg. Chem.* **2000**, *626*, 588−596.

(29) (a) *Ferrocenes: Ligands, Materials and Biomolecules*; Stepnicka, P., Ed.; John Wiley & Sons, Ltd.: Chichester, England, 2008; p 655. (b) Koslova, I. K.; Luk'yanov, O. A.; Tartakovskii, V. A. *Izv. Akad. Nauk SSSR, Ser. Khim.* **1981**, 2563−2571.

(30) (a) Engel, M. K.; Yao, J.; Maki, H.; Takeuchi, H.; Yonehara, H.; Pac, C. *Rep. Kawamura Inst. Chem. Res.* **1997**, *9*, 53−128. (b) Tippmann, E. M.; Schultz, P. G. *Tetrahedron* **2007**, *63*, 6182−6184. (c) Kato, T.; Tham, F. S.; Boyd, P. D. W.; Reed, C. A. *Heteroatom Chem.* **2006**, *17*, 209−216.

(31) (a) Ona-Burgos, P.; Casimiro, M.; Fernandez, I.; Navarro, A. V.; Fernandez Sanchez, J. F.; Carretero, A. S.; Gutierrez, A. F. *Dalton Trans.* **2010**, *39*, 6231−6238. (b) Koyama, T.; Suzuki, T.; Hanabusa, K.; Shirai, H.; Kobayashi, N. *Inorg. Chim. Acta* **1994**, *218*, 41−45. (c) Abraham, R. J.; Medforth, C. J. *Magn. Reson. Chem.* **1988**, *26*, 803−812. (d) Nemykin, V. N.; Kobayashi, N.; Chernii, V. Y.; Belsky, V. K. *Eur. J. Inorg. Chem.* **2001**, 733−743. (e) Nemykin, V. N.; Polshina, A. E.; Chernii, V. Y.; Polshin, E. V.; Kobayashi, N. *Dalton Trans.* **2000**, 1019−1025.

(32) (a) Claessens, C. G.; Gonzalez-Rodriguez, D.; Torres, T. *Chem. Rev.* **2002**, *102*, 835−853. (b) Kobayashi, N. In *The Porphyrin Handbook*; Kadish, K. M., Smith, K. M., Guilard, R., Eds.; Academic Press: New York, 2003; Vol. *15*, pp 161−262.

(33) Nemykin, V. N.; Makarova, E. A.; Grosland, J. O.; Hadt, R. G.; Koposov, A. Y. *Inorg. Chem.* **2007**, *46*, 9591−9601.

(34) (a) Gonzalez-Rodriguez, D.; Martinez-Diaz, M. V.; Abel, J.; Perl, A.; Huskens, J.; Echegoyen, L.; Torres, T. *Org. Lett.* **2010**, *12*, 2970−2973. (b) Sakamoto, K.; Ohno-Okumura, E. *Materials* **2009**, *2*, 1127−1179. (c) Camerel, F.; Ulrich, G.; Retailleau, P.; Ziessel, R. *Angew. Chem., Int. Ed.* **2008**, *47*, 8876−8880. (d) Iglesias, R. S.; Claessens, C. G.; Herranz, M. A.; Torres, T. *Org. Lett.* **2007**, *9*, 5381−5384. (e) Iglesias, R. S.; Claessens, C. G.; Torres, T.; Herranz, M. A.; Ferro, V. R.; Garcia de la Vega, J. M. *J. Org. Chem.* **2007**, *72*, 2967−2977.

(35) (a) Galangau, O.; Dumas-Verdes, C.; Schmidt, E. Y.; Trofimov, B. A.; Clavier, G. *Organometallics* **2011**, *30*, 6476−6481. (b) Herber, R. H.; Nowik, I.; Grosland, J. O.; Hadt, R. G..; Nemykin, V. N. *J. Organomet. Chem.* **2008**, *693*, 1850−1856. (c) Nemykin, V. N.; Maximov, A. Y.; Koposov, A. Y. *Organometallics* **2007**, *26*, 3138−3148. (d) Nemykin, V. N.; Olsen, J. G.; Perera, E.; Basu, P. *Inorg. Chem.* **2006**, *45*, 3557−3568. (e) Nemykin, V. N.; Hadt, R. G. *Inorg. Chem.* **2006**, *45*, 8297−8307. (f) Li, Y. L.; Han, L.; Mei, Y.; Zhang, J. Z. H. *Chem. Phys. Lett.* **2009**, *482*, 217−222. (g) Fabrizi de Biani, F.; Manca, G.; Marchetti, L.; Leoni, P.; Bruzzone, S.; Guidotti, C.; Atrei, A.; Albinati, A.; Rizzato, S. *Inorg. Chem.* **2009**, *48*, 10126−10137. (h) Li, F.; Sa, R.; Wu, K. *Mol. Phys.* **2008**, *106*, 2537−2544. (I) Santi, S.; Orian, L.; Donoli, A.; Durante, C.; Bisello, A.; Ganis, P.; Ceccon, A.; Crociani, L.; Benetollo, F. *Organometallics* **2007**, *26*, 5867−5879. (j) Zhang, W.-W.; Yu, Y.-G.; Lu, Z.-D.; Mao, W.-L.; Li, Y.-Z.; Meng, Q.-J. *Organometallics* **2007**, *26*, 865−873. (k) Parac, M.; Grimme, S. *J. Phys. Chem. A* **2002**, *106*, 6844−6850.

(36) (a) Lamsabhi, A. M.; Yanez, M.; Mo, O.; Trujillo, C.; Blanco, F.; Alkorta, I.; Elguero, J.; Caballero, E.; Rodriguez-Morgade, M. S.; Claessens, C. G.; Torres, T. *J. Porphyrins Phthalocyanines* **2011**, *15*, 1220−1230. (b) Xue, Z. L.; Mack, J.; Lu, H.; Zhang, L.; You, X. Z.; Kuzuhara, D.; Stillman, M.; Yamada, H.; Yamauchi, S.; Kobayashi, N. *Chem.—Eur. J.* **2011**, *17*, 4396−4407. (c) Jakubikova, E.; Campbell, I. H.; Martin, R. L. *J. Phys. Chem. A* **2011**, *115*, 9265−9272. (d) Zhong, A.; Zhang, Y.; Bian, Y. *J. Mol. Graph. Model.* **2010**, *29*, 470−480. (e) Mack, J.; Kobayashi, N.; Stillman, M. J. *J. Inorg. Biochem.* **2010**, *104*, 310−317. (f) Quartarolo, A. D.; Lanzo, I.; Sicilia, E.; Russo, N. *Phys. Chem. Chem. Phys.* **2009**, *11*, 4586−4592. (g) Eriksson, E. S. E.; Eriksson, L. A. *Phys. Chem. Chem. Phys.* **2011**, *13*, 7207−7217. (h) Galinato, M. G. I.; Spolitak, T.; Ballou, D. P.; Lehnert, N. *Biochemistry* **2011**, *50*, 1053−1069. (i) Uoyama, H.; Kim, K. S.; Kuroki, K.; Shin, J.-Y.; Nagata, T.; Okujima, T.; Yamada, H.; Ono, N.; Kim, D.; Uno, H. *Chem.—Eur. J.* **2010**, *16*, 4063−4074.

(37) Gouterman, M. *J. Mol. Spectrosc.* **1961**, *6*, 138−163.

(38) (a) Stuzhin, P. A.; Pimkov, I. V.; Ul'Khak, A.; Ivanova, S. S.; Popkova, I. A.; Volkovich, D. I.; Kuz'mitskii, V. A.; Donzello, M.-P. *Russ. J. Org. Chem.* **2007**, *43*, 1854−1863. (b) Matsushita, O.; Muranaka, A.; Kobayashi, Y.; Kobayashi, N. *Heterocycles* **2007**, *74*, 321−329. (c) Maslov, V. G. *Opt. Spectrosc.* **2006**, *101*, 853−861. (d) Kobayashi, N.; Nakajima, S.-I.; Ogata, H.; Fukuda, T. *Chem.—Eur. J.* **2004**, *10*, 6294−6312. (e) Stillman, M.; Mack, J.; Kobayashi, N. *J. Porphyrins Phthalocyanines* **2002**, *6*, 296−300. (f) Zhang, X.-B.; Feng, J.-K.; Ren, A.-M.; Sun, C.-C. *THEOCHEM* **2006**, *767*, 165−173. (g) Mack, J.; Stillman, M. J. *J. Porphyrins Phthalocyanines* **2001**, *5*, 67−76.

(39) (a) Tokura, S.; Sato, T.; Tsuneda, T.; Nakajima, T.; Hirao, K. *J. Comput. Chem.* **2008**, *29*, 1187−1197. (b) Chiba, M.; Fedorov, D. G.; Kitaura, K. *J. Chem. Phys.* **2007**, *127*, 104108−104118. (c) Seth, M.; Ziegler, T. *J. Chem. Phys.* **2006**, *124*, 144105−1441016. (d) Tawada, Y.; Tsuneda, T.; Yanagisawa, S.; Yanai, T.; Hirao, K. *J. Chem. Phys.* **2004**, *120*, 8425−8433. (e) Hirata, S.; Zhan, C.-G.; Apra, E.; Windus, T. L.; Dixon, D. A. *J. Phys. Chem. A* **2003**, *107*, 10154−10158.

(40) Lahmani, F.; Tramer, A.; Tric, C. *J. Chem. Phys.* **1974**, *60*, 4431−4447.